Smart Structures and Systems, *Vol. 27, No. 6 (2021) 1011-1029*
DOI: https://doi.org/10.12989/sss.2021.27.6.1011

Control performance of sloped rolling-type isolators designed with stepwise variable parameters

Shiang-Jung Wang* and Yi-Lin Sung [a]

Department of Civil and Construction Engineering, National Taiwan University of Science and Technology, No.43, Sec.4, Keelung Rd., Taipei 106335, Taiwan

(*Received September 9, 2020, Revised February 10, 2021, Accepted March 2, 2021*)

Abstract. With the same horizontal acceleration control performance, the horizontal displacement control performances of sloped rolling-type seismic isolators passively provided with stepwise variable parameters, as well as constant ones, are numerically investigated in this study. The first design possesses a smaller sloping angle with larger damping force at smaller horizontal isolation displacement and a larger sloping angle with smaller damping force at larger horizontal isolation displacement. In other words, this design has stepwise increased sloping angles and stepwise decreased damping force with increasing horizontal isolation displacement. The second design has an opposite design philosophy to the first one, i.e., it has stepwise decreased sloping angles and stepwise increased damping force with increasing horizontal isolation displacement. A series of numerical results present that for sloped rolling-type seismic isolators designed with a constant sloping angle and damping force, in general, the larger the damping force (in other words, the smaller the sloping angle), the smaller and the larger the horizontal maximum and residual displacement responses presented, respectively. The first and second designs with stepwise variable parameters each have its advantage for suppressing horizontal isolation displacement under far-field and pulse-like near-fault ground motions because of their larger energy dissipation capabilities designed at different stages. When the horizontal isolation displacement responses at the end of ground motions are still within the first slope rolling range with a larger sloping angle of the second design, as expected, adopting the second design can exhibit a better re-centering performance than adopting the first design. To have acceptable displacement control performances and without scarifying acceleration control performances under diverse seismic demands, compared with adopting the designs with constant parameters and the first design, adopting the second design could be an alternative solution and better choice.

Keywords: sloped rolling-type seismic isolator; stepwise variable; sloping angle; damping force; isolation displacement; residual displacement; near-fault

1. Introduction

Sloped rolling-type seismic isolators feature a constant horizontal acceleration control (or zero post-elastic stiffness) performance and an inherent gravity-based self-centering capability (Harvey and Kelly 2016). Although their in-plane seismic isolation performance has already been numerically and experimentally demonstrated in many past researches (Tsai *et al*. 2007, Lee *et al*. 2010, Wang *et al*. 2014, 2017), their sloping angle and damping force were usually designed as a constant, which might not really achieve their better passive control performances at different stages (or displacement levels) considered. This kind of demand is particularly important and necessary to be considered for some specific industries such as high-tech factories (Ghobarah 2001, Hwang *et al*. 2004), if different seismic performances or protective objectives are required under different levels of external disturbance, such as under frequent and catastrophic earthquakes or far-field and pulse-like near-fault ground motions whose seismic characteristics and caused responses are quite different (Baker 2007, Chopra and Chintanapakdee 2014). As Wang *et al*.'s previous numerical and statistical study indicated (Wang *et al*. 2019), as shown in Fig. 1, without remaining the same horizontal acceleration control performance, in general, the larger the designed sloping angle and damping force, in particular of the latter, the smaller the resulted horizontal isolation displacement. However, it can be clearly observed from the derived simplified equation of motion for the horizontal dynamic behavior of sloped rolling-type seismic isolators, when the roller is in motion on a sloped surface (Wang *et al*. 2014, 2017, 2019), an increase in sloping angles and damping force, evidently, will lead to larger horizontal acceleration transmitted to the protected object above the isolator. In other words, although increasing sloping angles and damping force can effectively mitigate horizontal isolation displacement, doing so, meanwhile, will also sacrifice the horizontal acceleration control performance. Moreover, an increase in damping force to suppress horizontal isolation displacement under major earthquakes might cause sloped rolling-type seismic isolators to have unacceptable self-centering performances under the earthquakes and even under other frequent or

*Corresponding author, Associate Professor,
E-mail: sjwang@mail.ntust.edu.tw
[a] Graduate Student, E-mail: m10705323@mail.ntust.edu.tw

ISSN: 1738-1584 (Print), 1738-1991 (Online)

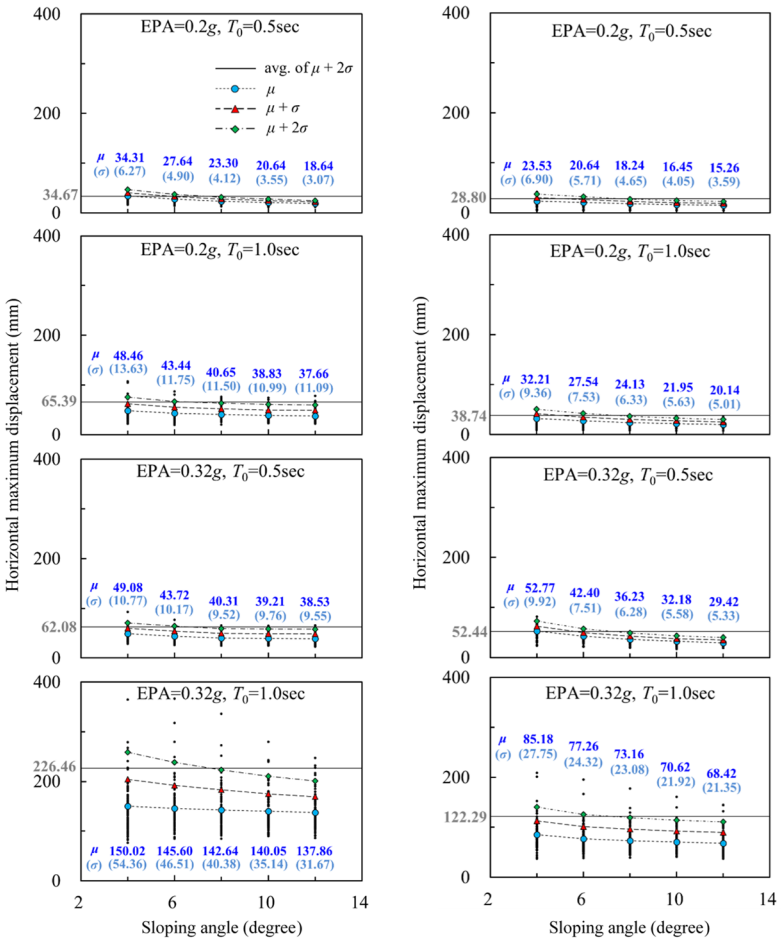

(a) $F_D = 0.1W$ (b) $F_D = 0.15W$

Fig. 1 Statistical horizontal maximum displacement responses of sloped rolling-type seismic isolators designed with sloping angles varying from 4 degrees to 12 degrees as well as damping force (F_D) equal to 10% and 15% of payload (W) under seismic demands with different effective peak acceleration (EPA) and corner period (T_0) (Wang *et al*. 2019)

minor earthquakes (Wang *et al*. 2014, 2019). It will quite often affect the serviceability and functionality of the protected object, which is undesirable especially for earthquake-prone zones.

Makris and Chang (Makris and Chang 2000, Chang *et al*. 2002) examined the efficiency of various dissipative mechanisms for protecting seismically isolated structures from near-fault pulse-like ground motions. It was concluded that compared with viscous damping, adopting friction damping could be more effective in reducing displacement demands and suppressing displacement amplification triggered by long duration pulses. It was particularly evident when the pulses had duration close to the designed isolation period. However, friction damping might be responsible for substantial permanent displacement occasionally. In addition to identifying a suitable range of optimum friction coefficients designed for friction-type dampers or seismic isolators against some specific ground motions considered (Jangid 2017), without sacrificing the acceleration control performance in most relevant researches, several variable friction damping mechanisms in passive and semi-active control manners, together with semi-active control algorithms, have been proposed to effectively reduce the displacement responses, including maximum and residual ones, of seismic isolation systems subjected to different ground motions.

Tadjbakhsh and Lin (1987) developed a passive control mechanism which can progressively increase frictional resistance by further tightening a set of friction plates. It was numerically demonstrated that compared with the constant frictional resistance design, adopting the proposed mechanism can have more reductions in acceleration transmissibility and relative displacement transmissibility. One of often seen passive control cases in the past two decades, which has already been widely applied in engineering practice as well, is the development of double and triple friction pendulum bearings (Fenz and Constantinou 2006, 2008, Abdollahzadeh and Darvishi 2017, Shahbazi and Taghikhany 2017, Yurdakul and Ates 2018). In addition to adopting different friction coefficients to present variable energy dissipation capabilities, varying curvature radii to present different stiffness (restoring force) capabilities was also adopted to offer designers greater flexibility to optimize the performances of friction pendulum bearings at different design stages as much as possible. Besides, the residual displacement responses of

double friction pendulum bearings designed with different friction coefficients together with their accumulation conditions were also numerically and experimentally investigated (Ponzo *et al*. 2017). Panchal and Jangid (2008) proposed an advanced base isolator in a passive control manner, i.e., variable friction pendulum systems. The variation of designed friction coefficients was such that up to a certain value of displacement the frictional force increased and then it decreased with further increase in displacement. The numerical results showed that the variable friction pendulum systems were very effective in controlling the responses of seismically isolated buildings under near-fault ground motions. Calvi *et al*. (2008) numerically studied the seismic performance of flat and curved sliding bearings for which different sliding materials with different frictional properties were designed. It was numerically demonstrated that the seismic isolators designed with variable damping may represent an improvement on the conventional seismic isolation solutions, in light of their higher energy absorption capacity, which contributed to significantly enhance their performance.

Feng *et al*. (1993) experimentally and analytically studied a hybrid sliding base isolation system composed of friction-controllable bearings. Some corresponding control algorithms and their effectiveness were developed and verified, respectively. For friction-type dampers, He *et al*. (2003) proposed semi-active friction control strategies which were capable of maintaining their motion in the slipping phase as much as possible together with eliminating undesirable acceleration spikes by introducing an appropriate boundary layer. The numerical results indicated that the proposed strategies were very effective. Narasimhan and Nagarajaiah (2006) proposed a control algorithm for reducing the seismic responses of base-isolated buildings equipped with variable friction semi-active control systems under near-fault ground motions. In addition, a new variable friction device consisting of four friction elements and four restoring spring elements arranged in a rhombus configuration with each arm consisting of a friction-stiffness pair was developed. The level of friction force can be adjusted by varying the angle of the arms of the device, thus leading to smooth variation of friction force in the device. The robustness of the proposed control algorithm and the developed device were experimentally demonstrated. Ozbulut and Hurlebaus (2010) developed two fuzzy logic controllers for operating the control force of piezoelectric friction dampers used in base isolation systems subjected to various ground motions. It was numerically verified that adopting the proposed controllers can effectively reduce isolation displacement without losing the potential advantage of acceleration control compared with the conventional base isolation design. Ozbulut *et al*. (2011) proposed two semi-active control strategies, the adaptive fuzzy neural controller and the direct adaptive control approach based on the simple adaptive control method, for variable friction dampers employed in seismic isolation systems. The numerical results revealed that the developed controllers can successfully improve the seismic response of base-isolated buildings against various ground motions. Chen and Wang (2016) proposed a novel mechanism, i.e., controllable embedded electromagnets, for enhancing the seismic performance of sloped rolling-type seismic isolators, and verified its efficacy through a series of shaking table tests. Without increasing the acceleration response transmitted to the protected object, it was experimentally and numerically demonstrated that simply adopting a switching control algorithm, i.e., applying additional damping force only when the roller is in motion toward to the original position, had a better isolation displacement control performance than the conventional isolator. More importantly, it had a comparable and even superior control performance to the isolator equipped with controllable embedded electromagnets but applying other more complicated control algorithms. Iemura *et al*. (2019) developed an autonomous semi-active control law which was intended to minimize the disadvantages of friction-type dampers, including residual displacement and generated high-frequency damping force. The numerical results presented that the proposed control law was effective for a variety of ground motions.

In addition to varying friction damping, some variable stiffness mechanisms in passive and semi-active control manners for seismic isolation design have been developed and studied. The double or triple friction pendulum bearing aforementioned (Fenz and Constantinou 2006, 2008), of course, is one of often seen passive control cases. In Lu *et al*.'s study (2013), to achieve multiple design objectives, the idea of polynomial friction pendulum isolators with variable stiffness properties was proposed and investigated. After experimentally verifying the design idea, the numerical results presented that applying the isolators to a floor isolation system did comply with the dual performance objectives as expected. Moreover, Lu *et al*. (2008) proposed a sliding base isolation system whose stiffness property was controllable. Thus, the restoring force provided by the system can then be controlled by a semi-active control method developed based on the active feedback control concept. The numerical results indicated that adopting the proposed system and control method can effectively control both isolation displacement and transmitted acceleration responses. Narasimhan and Nagarajaiah (2005) developed a new short time Fourier transformation control algorithm for reducing the seismic responses of buildings isolated with a variable stiffness system under near-fault ground motions. The test results of a five-story reinforced concrete building isolated with elastomeric bearings and a variable stiffness system presented that the controller whose stiffness was simply varied a few times was effective enough in reducing isolation displacement and even story drifts without increasing acceleration responses. Since controlling variable stiffness for conventional seismic isolators might be too complicated to be implemented in most applications, Liu *et al*. (2008) proposed a new system in a configuration of two controllable magnetorheological fluid dampers and two constant springs. The equivalent stiffness of the whole system was varied by controlling the damper in the Voigt element, and its variable damping was controlled by the second damper parallel to the other elements. The experimental results showed that the proposed system with

damping and stiffness on-off control can exhibit an excellent vibration isolation performance for a broad range of excitations.

In this study, to keep the unique feature of sloped rolling-type seismic isolators, i.e., the constant horizontal acceleration performance when the roller is in motion on a sloped surface, passively stepwise variable sloping angles and damping force, rather than other more complicated passive or even semi-active control mechanisms, are implemented into the isolators. In this case, the revealed hysteretic behavior, basically, is similar to the one of applying the switching control algorithm to sloped rolling-type seismic isolators equipped with controllable embedded electromagnets (Chen and Wang 2016) and a smart base-isolated raised floor system composed of sloped rolling-type seismic isolators and magnetorheological (MR) dampers (Chen *et al*. 2019). Nevertheless, and most importantly, the control mechanism proposed in this study is relatively simple and passive-based. Through conducting numerical study under a large number of ground motions with different seismic characteristics, the horizontal displacement control performances of the two different design philosophies are compared and discussed. It is emphasized that with a given constant horizontal acceleration control performance, numerically comparing seismic responses of sloped rolling-type seismic isolators designed with stepwise variable and constant parameters, rather than seeking their optimum design parameters, is the main purpose of this study.

2. Design concept

2.1 Analytical model

Based on the simplified model in which a roller is in motion between a sloped surface and a flat surface as illustrated in Fig. 2(a), the simplified and linearized equation of motion for the horizontal dynamic behavior of sloped rolling-type seismic isolators can be obtained by Eq. (1) (Wang *et al*. 2014, 2017, 2019), and its typical hysteretic behavior without considering the effect of $\ddot{z}_g$ is shown in Fig. 2(b).

$$\ddot{x} + \ddot{x}_g = \frac{-(g + \ddot{z}_g)\theta}{2} sgn(x) - \frac{F_D}{(M + m_1)} sgn(\dot{x}) \quad (1)$$

where $\ddot{x}(x)$ is the horizontal acceleration (displacement) response of the protected object and the bearing plate above the roller (or the superior bearing plate as indicated in Fig. 2(a)) relative to the fixed base; $\ddot{x}_g$ and $\ddot{z}_g$ are the horizontal and vertical acceleration excitations, respectively; g is the acceleration of gravity; θ is the sloping angle of the V-shaped surface of either bearing plate in contact with the roller (e.g., the inferior bearing plate as indicated in Fig. 2(a)); F_D is the horizontal friction damping force, which is simplified as a dry friction problem in this study rather than a relatively complex model that can further considering the effects of bilateral disturbance, velocity, axial pressure, temperature, breakaway friction, and others (Constantinou *et al*. 1990, Kumar *et al*. 2015,

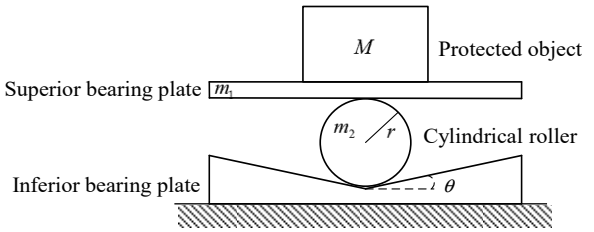

(a) Simplified model

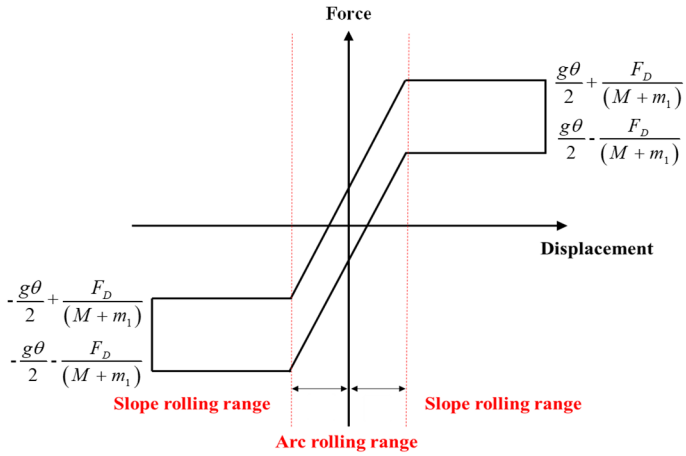

(b) Hysteretic behavior

Fig. 2 A model simply considering a roller in motion between sloped and flat surfaces and its typical hysteretic behavior

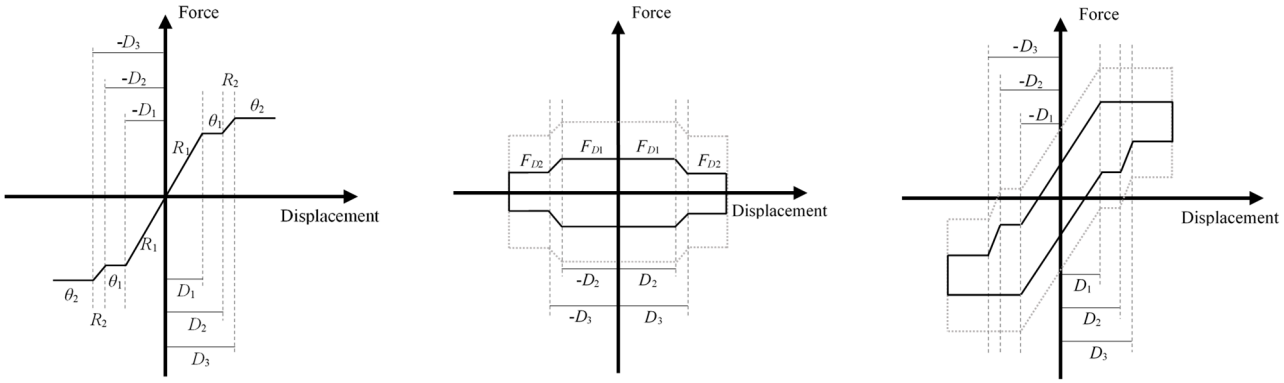

(a) Multi-linear elastic behavior (b) Hysteretic behavior (c) Combined (a) and (b) behavior

Fig. 3 Illustrations of displacement-force relation of Design I

Wei *et al*. 2017); M, m_1, and m_2 are the seismic reactive masses of the protected object, superior bearing plate, and roller, respectively; and r is the sectional radius of the roller.

In this study, sloped rolling-type seismic isolators are intended to be provided with stepwise variable sloping angles and damping force. For keeping their unique feature, i.e., with the same horizontal acceleration control performance at different stages (or displacement levels), which is different from the assumption made in Wang *et al*.'s previous study (2019), two patterns are designed and numerically examined. As for the first design pattern, denoted as Design I hereafter, the sloping angle of the V-shaped surface in contact with the roller becomes larger stepwise while the damping force becomes smaller stepwise with increasing horizontal isolation displacement. To prevent pounding when the roller is passing through the sharp angle of the V-shaped surface and moving from one slope to another discontinuous slope, an arc rolling range (or called a transition range) with a fixed curvature radius is designed (Wang *et al*. 2014). The multi-linear elastic behavior considering two sloping angles stepwise increased with increasing horizontal isolation displacement (or called slope rolling ranges) and two transition ranges (or called arc rolling ranges), for instance, is illustrated in Fig. 3(a), in which D_1 is the first transition range designed with a fixed curvature radius R_1; D_1 to D_2 is the first slope rolling range designed with a sloping angle θ_1 between the first and second transition ranges; D_2 to D_3 is the second transition range designed with a fixed curvature radius R_2 between the first and second slope rolling ranges; and D_3 to the designed maximum horizontal isolation displacement capacity is the second slope rolling range designed with a sloping angle θ_2 ($> \theta_1$).

In the first transition range, the damping force is designed to be identical to that in the first slope rolling range. In the second transition range, the damping force is accordingly designed to be linearly varied. Corresponding to Fig. 3(a), the hysteretic behavior considering two damping force stepwise decreased with increasing horizontal isolation displacement and one transition range in between (i.e., the second transition range) is illustrated in Fig. 3(b), in which F_{D1} is the damping force magnitude designed in the first transition and slope rolling ranges, i.e., D_2; F_{D2} ($< F_{D1}$) is the damping force magnitude designed in the second slope rolling range, i.e., after D_3; and the damping force is linearly varied from F_{D1} to F_{D2} with increasing horizontal isolation displacement in the second transition range, i.e., D_2 to D_3. The representative horizontal hysteretic behavior of Design I with two stepwise increased sloping angles and two stepwise decreased damping force with increasing horizontal isolation displacement, i.e., the combination of Figs. 3(a)-(b), is presented in Fig. 3(c). Note that with a greater damping force design, more horizontal hysteretic loop areas will be presented in the second and

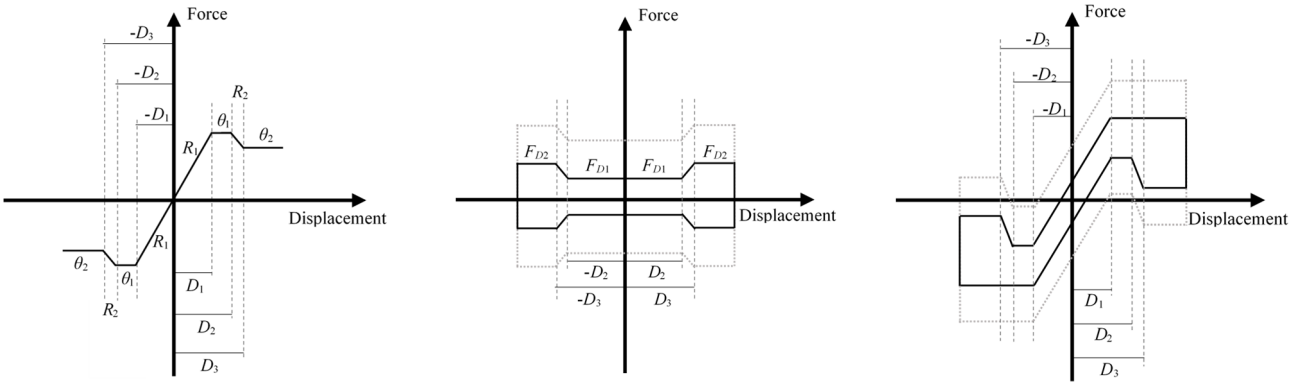

(a) Multi-linear elastic behavior (b) Hysteretic behavior (c) Combined (a) and (b) behavior

Fig. 4 Illustrations of displacement-force relation of Design II

fourth quadrants, as indicated by dash and gray lines shown in Figs. 3(b)-(c).

When the roller is in motion in the slope rolling ranges (e.g., D_1 to D_2 and after D_3 as shown in Fig. 3) and in the arc rolling ranges (e.g., D_1 and D_2 to D_3 as shown in Fig. 3), the horizontal dynamic behavior of Design I can be characterized by the simplified equations of motion as given in Eqs. (1)-(2), respectively (Wang *et al*. 2014, 2017, 2019).

$$\ddot{x} + \ddot{x}_g = -\frac{g}{4R}x - \frac{F_D}{(M+m_1)}sgn(\dot{x}) \quad (2)$$

where R is the curvature radius of the round surface.

As for the second design pattern, denoted as Design II hereafter, the sloping angle of the V-shaped surface in contact with the roller becomes smaller stepwise while the damping force becomes larger stepwise with increasing horizontal isolation displacement. An arc rolling range (or called a transition range) with a fixed curvature radius is designed between two discontinuous slopes. In contrast with Fig. 3(a), the multi-linear elastic behavior considering two sloping angles stepwise decreased with increasing horizontal isolation displacement (or called slope rolling ranges) and two transition ranges (or called arc rolling ranges) is illustrated in Fig. 4(a), in which the definitions of all the notations are identical to those shown in Fig. 3(a) except that θ_2 is smaller than θ_1. In the first transition range, the damping force is designed to be identical to that in the first slope rolling range. In the second transition range, the damping force is accordingly designed to be linearly varied. In contrast with Fig. 3(b), the hysteretic behavior considering two damping force stepwise increased with increasing horizontal isolation displacement and one transition range in between (i.e., the second transition range) is illustrated in Fig. 4(b), in which the definitions of all the notations are identical to those in Fig. 3(b) except that F_{D2} is larger than F_{D1}. The representative horizontal hysteretic behavior of Design II with two stepwise decreased sloping angles and two stepwise increased damping force with increasing horizontal isolation displacement, i.e., the combination of Figs. 4(a) and 4(b), is presented in Fig. 4(c). Note that with a greater damping force design, more horizontal hysteretic loop areas will be presented in the second and fourth quadrants, as indicated by dash and gray lines shown in Figs. 4(b)-(c). Similarly, when the roller is in motion between a sloped surface and a flat surface as well as between a round surface and a flat surface, the horizontal dynamic behavior of Design II can be characterized by the simplified equations of motion as given in Eqs (1)-(2), respectively (Wang *et al*. 2014, 2017, 2019).

2.2 Practical feasibility in mechanical design

2.1.1 Stepwise variable sloping angles

As described previously, the transition range when the roller is passing through two discontinuous slopes with different sloping angles, e.g., D_1 and D_2 to D_3 as shown in Figs. 3(a) and 4(a), is mechanically realized by designing an arc rolling range, as illustrated in Figs. 5(a)-(b) for Design I and Design II, respectively. This mechanical design idea has already been successfully implemented in Wang *et al*.'s previous experimental researches (Wang *et al*. 2014, 2017), in order to prevent pounding when the roller is passing through the sharp angle of the V-shaped surface. A series of test results demonstrated that adopting this method not only can achieve the desired performance but can mechanically exhibit the linearly elastic behavior, which can be simply characterized by the designed curvature radius of the round surface in the arc rolling range. Therefore, the design concept of stepwise variable sloping angles, either increased (i.e., Design I) or decreased (i.e., Design II) with increasing horizontal isolation displacement proposed in this study, is mechanically and practically feasible.

2.1.2 Stepwise variable damping force

In Wang *et al*.'s previous experimental research (Wang *et al*. 2020), a mechanism to design sloped rolling-type

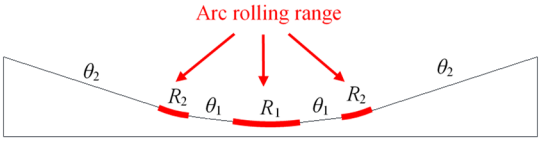

(a) Stepwise variable sloping angles (Design I)

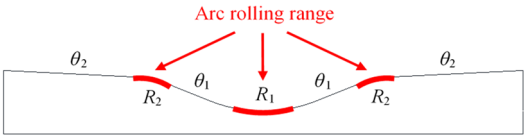

(b) Stepwise variable sloping angles (Design II)

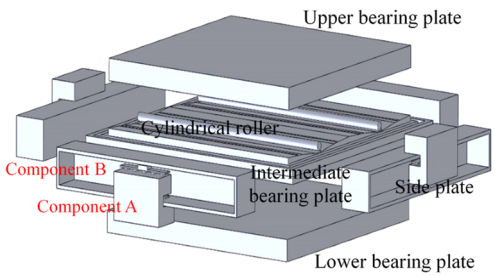

(c) Whole model

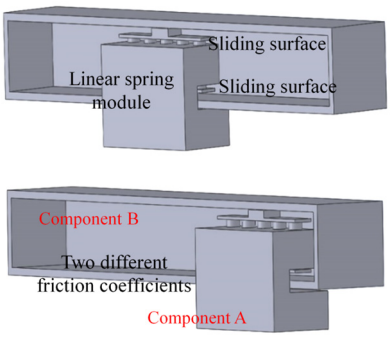

(d) Stepwise variable damping force

Fig. 5 Illustrations of mechanical design of stepwise variable sloping angles and damping force

seismic isolators with linearly variable friction damping force was proposed and experimentally examined. Herein, the previous mechanism is modified slightly to have a stepwise variable damping force performance. The whole model is illustrated in Fig. 5(c), which is still composed of bearing plates (including upper, intermediate, and lower ones), side plates, and cylindrical rollers (Wang *et al*. 2014). In one horizontal principle direction and on one side surface of any bearing plate, there are two major, mutually holding components (i.e., side plates) of which one is attached to the upper (or lower) bearing plate, denoted as Component A, and other one is attached to the intermediate bearing plate, denoted as Component B. Accordingly, there are two sliding motions in parallel, rather than one sliding motion, between Components A and B under external disturbance. In other words, Component A or B has two sliding surfaces respectively directed upward and downward. By means of this modified mechanism, the stability of sloped rolling-type seismic isolators can also be significantly improved compared with the conventional model (Wang *et al*. 2014).

By installing the same sets of linear spring modules with identical initial shortening behind the two sliding surfaces of Component A, the two sliding surfaces of Component A are always in contact with the two sliding surfaces of Component B. There always exist action and reaction force between Components A and B), regardless of being at the equilibrium position or in motion, as illustrated in Fig. 5(d). When the horizontal motion of Component A relative to Component B, which is equal to the horizontal isolation displacement of the sloped rolling-type seismic isolator, becomes larger, Component A attached to the upper (lower) bearing plate will move upward (downward) relative to Component B attached to the intermediate bearing plate. Therefore, the resultant friction damping force contributed by the two sliding motions will be remained as a constant. It is because the linear spring modules behind the two sliding surfaces of Component A are respectively further compressed and released with the same quantity so as to correspondingly produce larger and smaller normal force. In other words, the differences in the deformation (or the produced normal force) of the linear spring modules behind the two sliding surfaces of Component A will be automatically canceled out during motion.

To further make the modified mechanism afore-mentioned exhibit stepwise variable damping force, for instance, two damping force stepwise decreased and increased with increasing horizontal isolation displacement correspondingly shown in Figs. 3(b) and 4(b), the two sliding surfaces of Component B are designed to have two ranges with different kinetic friction coefficients, as illustrated in Fig. 5(d). This design concept is similar to the idea proposed in Calvi *et al*.'s study (2008). As for Design I shown in Fig. 3(b), the first and second ranges of the two sliding surfaces of Component B, i.e., the ranges varying from the equilibrium position to D_2 and from D_2 to the designed maximum horizontal isolation displacement capacity, are correspondingly designed with a larger and a smaller kinetic friction coefficient so as to produce F_{D1} and F_{D2} in the first transition and slope rolling ranges as well as in the second slope rolling range, respectively. As for Design II shown in Fig. 4(b), the mechanical design concept is similar to that of Design I, except that the first and second ranges of the two sliding surfaces of Component B are correspondingly designed with a smaller and a larger kinetic friction coefficient. The lengths of the two sliding surfaces of Component A are designed to be equal to the second transition range (i.e., $|D_3 - D_2|$) shown in Figs. 3(b) and 4(b). Therefore, the linearly variable damping force with increasing horizontal isolation displacement in the second transition range (i.e., $|D_3 - D_2|$), either decreased (i.e., Design I) as shown in Fig. 3(b) or increased (i.e., Design II) as shown in Fig. 4(b), can be realized through the process from when the two sliding surfaces of Component A begin contacting the second range of the two sliding surfaces of Component B to when those move completely in the second range.

3. Numerical study scheme

3.1 Design models

A to-be-protected object above the sloped rolling-type seismic isolators designed with stepwise variable parameters is assumed to possess a seismic reactive mass of 1000 kg. For simplicity, the external disturbance and dynamic responses in only one horizontal principle direction are considered. Thus, Eq. (1) can be further simplified as Eq. (3) herein. Besides, the surfaces of the superior and inferior bearing plates in contact with the roller, as illustrated in Fig. 2, are designed to be flat and V-shaped, respectively. Note that all the following models are designed to have the same maximum horizontal acceleration transmitted to the protected object. A value of 0.08 g, which is a commonly used design objective when adopting sloped rolling-type seismic isolators for protecting critical equipment in high-tech industries from malfunction during earthquakes, is assumed to be the maximum transmitted acceleration in this preliminary numerical study.

$$\ddot{x} + \ddot{x}_g = \frac{-g\theta}{2} sgn(x) - \frac{F_D}{(M + m_1)} sgn(\dot{x}) \tag{3}$$

Four Design I models are denoted as VSD-36A, VSD-48A, VSD-36B, and VSD-48B hereafter. VSD-36A, VSD-48A and VSD-36B, VSD-48B are designed to have the same first slope rolling range, i.e., $|D_2 - D_1|$ = 10 mm. Nevertheless, VSD-36A has a smaller sloping angle but larger damping force in both the first and second slope rolling ranges (i.e., θ_1 = 3 degrees, θ_2 = 6 degrees, F_{D1} = 550 N, and F_{D2} = 300 N) than VSD-48A (i.e., θ_1 = 4 degrees, θ_2 = 8 degrees, F_{D1} = 460 N, and F_{D2} = 120 N). The design parameters of VSD-36B and VSD-48B are almost identical to those of VSD-36A and VSD-48A, respectively, except that the first slope rolling range for VSD-36B and VSD-48B, i.e., D_1 to D_2, is designed as a larger value. That is, $|D_2 - D_1|$ = 20 mm for VSD-36B and VSD-48B. Once the curvature radii in the first and second transition ranges are determined (i.e., R_1 = 100 mm and R_2 = 50 mm, respectively), the different ranges, i.e., D_1, D_2, and D_3, for

Table 1 Design parameters of different models

Design I (stepwise increased sloping angles and stepwise decreased damping force)								
	First transition (or arc rolling) range		First slope rolling range		Second transition (or arc rolling) range		Second slope rolling range	
VSD-36A	D_1 (mm)	10.5	D_2 (mm)	20.5	D_3 (mm)	25.75		
	R_1 (mm)	100	θ_1 (degrees)	3	R_2 (mm)	50	θ_2 (degrees)	6
	F_{D1} (N)	550	F_{D1} (N)	550	F_{D1} (N)	550	F_{D2} (N)	300
					F_{D2} (N)	300		
VSD-48A	D_1 (mm)	14	D_2 (mm)	24	D_3 (mm)	31		
	R_1 (mm)	100	θ_1 (degrees)	4	R_2 (mm)	50	θ_2 (degrees)	8
	F_{D1} (N)	460	F_{D1} (N)	460	F_{D1} (N)	460	F_{D2} (N)	120
					F_{D2} (N)	120		
VSD-36B	D_1 (mm)	10.5	D_2 (mm)	30.5	D_3 (mm)	35.75		
	R_1 (mm)	100	θ_1 (degrees)	3	R_2 (mm)	50	θ_2 (degrees)	6
	F_{D1} (N)	550	F_{D1} (N)	550	F_{D1} (N)	550	F_{D2} (N)	300
					F_{D2} (N)	300		
VSD-48B	D_1 (mm)	14	D_2 (mm)	34	D_3 (mm)	41		
	R_1 (mm)	100	θ_1 (degrees)	4	R_2 (mm)	50	θ_2 (degrees)	8
	F_{D1} (N)	460	F_{D1} (N)	460	F_{D1} (N)	460	F_{D2} (N)	120
					F_{D2} (N)	120		
Design II (stepwise decreased sloping angles and stepwise increased damping force)								
	First transition (or arc rolling) range		First slope rolling range		Second transition (or arc rolling) range		Second slope rolling range	
VSD-63A	D_1 (mm)	21	D_2 (mm)	31	D_3 (mm)	36.25		
	R_1 (mm)	100	θ_1 (degrees)	6	R_2 (mm)	50	θ_2 (degrees)	3
	F_{D1} (N)	300	F_{D1} (N)	300	F_{D1} (N)	300	F_{D2} (N)	550
					F_{D2} (N)	550		
VSD-84A	D_1 (mm)	28	D_2 (mm)	38	D_3 (mm)	45		
	R_1 (mm)	100	θ_1 (degrees)	8	R_2 (mm)	50	θ_2 (degrees)	4
	F_{D1} (N)	120	F_{D1} (N)	120	F_{D1} (N)	120	F_{D2} (N)	460
					F_{D2} (N)	460		
VSD-63B	D_1 (mm)	21	D_2 (mm)	41	D_3 (mm)	46.25		
	R_1 (mm)	100	θ_1 (degrees)	6	R_2 (mm)	50	θ_2 (degrees)	3
	F_{D1} (N)	300	F_{D1} (N)	300	F_{D1} (N)	300	F_{D2} (N)	550
					F_{D2} (N)	550		
VSD-84B	D_1 (mm)	28	D_2 (mm)	48	D_3 (mm)	55		
	R_1 (mm)	100	θ_1 (degrees)	8	R_2 (mm)	50	θ_2 (degrees)	4
	F_{D1} (N)	120	F_{D1} (N)	120	F_{D1} (N)	120	F_{D2} (N)	460
					F_{D2} (N)	460		

Constant sloping angles and damping force					
	Transition (or arc rolling) range			Slope rolling range	
	D (mm)	R (mm)	F_D (N)	θ (degrees)	F_D (N)
CSD-3	10.5	100	550	3	550
CSD-4	14	100	460	4	460
CSD-6	21	100	300	6	300
CSD-8	28	100	120	8	120

VSD-36A, VSD-48A, VSD-36B, and VSD-48B can be calculated accordingly.

Four Design II models are denoted as VSD-63A, VSD-84A, VSD-63B, and VSD-84B hereafter. VSD-63A, VSD-84A and VSD-63B, VSD-84B are designed to have the same first slope rolling ranges as VSD-36A, VSD-48A (i.e., $|D_2 - D_1| = 10$ mm) and VSD-36B, VSD-48B (i.e., $|D_2 - D_1| = 20$ mm), respectively. Compared with VSD-84A and VSD-84B (i.e., $\theta_1 = 8$ degrees, $\theta_2 = 4$ degrees, $F_{D1} = 120$ N, and $F_{D2} = 460$ N), VSD-63A and VSD-63B have a smaller sloping angle but larger damping force in both the first and second slope rolling ranges (i.e., $\theta_1 = 6$ degrees, $\theta_2 = 3$ degrees, $F_{D1} = 300$ N, and $F_{D2} = 550$ N). Similarly, once the curvature radii in the first and second transition ranges are determined (i.e., $R_1 = 100$ mm and $R_2 = 50$ mm, respectively), the different ranges, i.e., D_1, D_2, and D_3, for VSD-63A, VSD-84A, VSD-63B, and VSD-84B can be calculated accordingly.

In addition to the eight models designed with stepwise variable sloping angles and damping force aforementioned, another four models designed with constant sloping angles and damping force are numerically analyzed as the counterparts, denoted as CSD-3, CSD-4, CSD-6, and CSD-8 hereafter. For objective comparison, i.e., to keep the same maximum horizontal acceleration transmitted to the protected object, the constant values of sloping angles and damping force (θ, F_D) designed for the four counterpart models in sequence are equal to (3 degrees, 550 N), (4 degrees, 460 N), (6 degrees, 300 N), and (8 degrees, 120 N). The curvature radius in the arc rolling range designed for CSD-3, CSD-4, CSD-6, and CSD-8, i.e., $R = 100$ mm, is identical to that in the first transition range designed for VSD-36A, VSD-48A, VSD-36B, VSD-48B, VSD-63A, VSD-84A, VSD-63B, and VSD-84B, i.e., $R_1 = 100$ mm. Note that the sloping angles and damping force designed for CSD-3 and CSD-6 are correspondingly equal to those designed for the first and second (second and first) slope rolling ranges of VSD-36A or VSD-36B (VSD-63A or VSD-63B), and those designed for CSD-4 and CSD-8 are correspondingly equal to those designed for the first and second (second and first) slope rolling ranges of VSD-48A or VSD-48B (VSD-84A or VSD-84B). Similarly, once the curvature radius in the arc rolling range is determined (i.e., $R = 100$ mm), the arc rolling range, i.e., D, for CSD-3, CSD-4, CSD-6, and CSD-8 can be calculated accordingly. The design parameters of VSD-36A, VSD-48A, VSD-36B, VSD-48B, VSD-63A, VSD-84A, VSD-63B, VSD-84B, CSD-3, CSD-4, CSD-6, and CSD-8 are detailed in Table 1.

3.2 External disturbance

Three groups of ground motion records are adopted as horizontal acceleration inputs. The first group (denoted as Group 1 hereafter) contains 2,553 sets of local ground

Table 2 Acceleration input program (* denotes the ground motions duplicated in Groups 1 and 2 (or 3))

	Earthquake	Year	Station name (denotation)	PGA (g)	PGV (m/s)	Earthquake	Year	Station name (denotation)	PGA (g)	PGV (m/s)
Group 1	-	1992~2006	-	0.082~1.260	0.006~2.800					
Group 2	El Centro	1940	American Imperial Valley	0.281	0.309	Japan Kobe	1995	Tadoka (000)	0.296	0.245
	American Imperial Valley	1979	Delta (352)	0.350	0.330			Kakogwa (000)	0.240	0.208
	American Superstition Hills	1987	Poe Road (270)	0.475	0.412			Shin-Osaka (090)	0.233	0.218
	American Whittier Narrows	1987	Beverly Hills (279)	0.140	0.104			MRG (000)	0.214	0.270
	American Loma Prieta	1989	Gilroy Array #3 (000)	0.559	0.363			Fukushima (000)	0.185	0.314
			Capitola (090)	0.439	0.296			Yae (000)	0.158	0.212
	Iran Manjil	1990	Abbar (L)	0.515	0.425	Turkey Kocaeli	1999	Duzce (270)	0.364	0.557
	American Landers	1992	Yermo Fire (360)	0.152	0.291			Arcelik (000)	0.210	0.140
	American Northridge	1994	Beverly Hills-12520 Mulhol (035)	0.621	0.288	Taiwan Chi-Chi	1999	TCU074 (EW)*	0.597	0.704
			Canyon Country (270)	0.472	0.411			TCU045 (NS)	0.522	0.46
			LA-Saturn St (020)	0.468	0.372			TCU088 (EW)*	0.519	0.137
			Glendale-Las Palmas (177)	0.365	0.113			TCU047 (NS)	0.407	0.333
			LA-Hollywood Stor FF (360)	0.358	0.274			NST (NS)	0.399	0.329
	Japan Kobe	1995	Nishi-Akashi (000)	0.483	0.468			TCU089 (EW)*	0.355	0.508

Table 2 Continued

	Earthquake	Year	Station name (denotation)	PGA (g)	PGV (m/s)	Earthquake	Year	Station name (denotation)	PGA (g)	PGV (m/s)
Group 3	American San Fernanado	1971	Pacoima Dam (upper left abut) (164)	1.129	1.144	Taiwan Chi-Chi	1999	TCU128 (EW)*	0.144	0.642
	American Superstition	1987	Parachute Test Site (225)	0.429	1.342	Turkey Kocaeli	1999	Yarimca (150)	0.320	0.719
	American Lexington Dam	1989	Los Gatos (000)	0.436	0.857			Yarimca (060)	0.226	0.697
			Los Gatos (090)	0.409	0.957	Iran_Bam	2003	Bam (L)	0.808	1.241
	American Cape Mendocino	1992	Petrolia (090)	0.605	0.885	New Zealand Darfield	2010	HORC (S72E)	0.472	0.698
	Turkey Erzincan	1992	Erzincan (NS)	0.385	1.071	Taiwan Meinong	2016	CHY063 (EW)*	0.425	0.693
	American Northridge	1994	Pacoima Dam (upper left) (194)	0.989	1.033			CHY089 (NS)	0.288	0.577
			Rinaldi (228)	0.869	1.479	Taiwan Hualien	2018	HWA019 (EW)*	0.411	1.384
			Sylmar-Converter Sta East (011)	0.851	1.209			HWA008 (NS)	0.343	0.861
			Sylmar-Olive View Med FF (360)	0.798	1.293			HWA014 (EW)*	0.324	1.465
			Sylmar-Converter Sta (052)	0.617	1.162			MND016 (EW)*	0.306	1.336
			Jensen Filter Plant Generator Building (022)	0.569	0.761			HWA007 (EW)*	0.295	1.034
	Japan Kobe	1995	KJMA (000)	0.834	0.911			HWA012 (EW)*	0.285	0.866
	Turkey Duzce	1999	Bolu (090)	0.806	0.659			HWA063 (NS)	0.258	0.997
	Taiwan Chi-Chi	1999	TCU067 (EW)*	0.498	0.983			HWA028 (NS)	0.258	0.517
			CHY101 (NS)	0.398	1.073			HWA009 (EW)*	0.255	1.104
			TCU052 (EW)*	0.357	1.746			HWA008 (EW)*	0.235	0.992
			CHY101 (EW)*	0.340	0.672			HWA 062 (EW)*	0.213	0.956
			TCU075 (EW)*	0.330	1.161			TRB 042 (EW)*	0.208	0.656
			TCU102 (EW)*	0.310	0.874			HWA062 (NS)	0.207	0.764
			CHY024 (EW)*	0.282	0.529			HWA011 (NS)	0.203	0.871
			TCU063 (EW)*	0.183	0.440			HWA050 (NS)	0.202	0.763
			TCU102 (NS)	0.172	0.713			TRB042 (NS)	0.190	0.826
			TCU128 (NS)	0.166	0.626					

motion records with peak ground acceleration (PGA) varying from 0.082 g to 1.260 g and peak ground velocity (PGV) varying from 0.006 m/s to 2.800 m/s. Those were collected by the Taiwan Strong Motion Instrument Program (TSMIP) during July 29th, 1992 to December 31st, 2006. Among these, 18 records are classified as pulse-like near-fault ground motions (Shahi and Baker 2014), and the remaining are classified as far-field ground motions. The second and third groups, correspondingly denoted as Group 2 and Group3 hereafter, contain 28 sets of far-field ground motion records and 47 sets of pulse-like near-fault ground motion records (Shahi and Baker 2014), respectively, during past global earthquakes. Those were collected by the Pacific Earthquake Engineering Research Center (PEER). The PGA and PGV values of ground motion records of Group 2 are varied from 0.140 g to 0.621 g and from 0.104 m/s to 0.704 m/s, respectively, and the PGA and PGV values of ground motion records of Group 3 are varied from 0.144 g to 1.129 g and from 0.440 m/s to 1.479 m/s, respectively. The basic information of these ground motions, including the earthquake, year of occurrence, station name (as the denotation hereafter), PGA, and PGV, is summarized in Table 2. Note that adopting Group 1 aims to more clearly identify the influences of different design

parameters on wide-ranging seismic response of sloped rolling-type seismic isolators, while adopting Groups 2 and 3 can further understand and compare the merits and demerits of different design models subjected to far-field and pulse-like near-fault ground motions. Thus, a few ground motions classified into Groups 2 and 3 are duplicated in Group 1.

3.3 Analysis program

In this study, MATLAB is adopted to develop the nonlinear response history analysis program for sloped rolling-type seismic isolators provided with constant and stepwise variable sloping angles and damping force. The Newmark-β method with linear acceleration is used for solving Eqs. (2)-(3) to obtain their horizontal dynamic responses in the arc and slope rolling ranges at each time step, respectively. By substituting different curvature radii (i.e., R_1 and R_2), sloping angles (i.e., θ_1 and θ_2), and damping force (i.e., F_{D1}, F_{D2}, and the linear variation in between (Wang *et al*. 2020)) into Eqs. (2)-(3), the horizontal dynamic behavior at different stages (i.e., D_1, D_2, D_3 and D_4) for both Design I and Design II models can be appropriately considered. The term $F_D(x)\,sgn(\dot{x})$ presented in Eqs. (2)-(3) correspondingly in the first transition and slope rolling ranges (i.e., when $|x| < D_2$), that presented in Eq. (3) in the second transition range (i.e., when $D_2 < |x| < D_3$), and that presented in Eq. (2) in the second slope rolling range (i.e., when $|x| > D_3$) are mathematically described by using Eqs. (4)-(6), respectively.

$$F_D(x)\,sgn(\dot{x}) = F_{D1}\,sgn(\dot{x}) \tag{4}$$

$$F_D(x)\,sgn(\dot{x}) = sgn(\dot{x})\left[F_{D1} + \frac{|x| - D_2}{(D_3 - D_2)}(F_{D2} - F_{D1})\right] \tag{5}$$

$$F_D(x)\,sgn(\dot{x}) = F_{D2}\,sgn(\dot{x}) \tag{6}$$

During two or more consecutive time steps in numerical integration, there might be no relative motion between the superior and inferior bearing plates as shown in Fig. 2(a). Therefore, the relative static state (or sticking phase) (He *et al*. 2003), which is the main cause of post-earthquake residual displacement of sloped rolling-type seismic isolators, is also taken into consideration in the analysis program. When setting $\ddot{x}$ in Eqs. (2)-(3) equal to zero, the critical characteristic strengths $F_{D,C}$ can be defined and calculated by Eqs. (7)-(8), respectively. If $F_{D,C}$ is calculated to be smaller than the designed damping force F_D at a specific time step (e.g., at t_i), the relative static state will occur. Under this circumstance, at the time step t_i, $\ddot{x}$ and $\dot{x}$ should be equal to zero, and x should remain the same as that at the previous time step t_{i-1}. Note that $F_{D,C}$ in the slope rolling range is only related to $\ddot{x}_g$ once θ is determined, while $F_{D,C}$ in the arc rolling range is also related to x, in addition to $\ddot{x}_g$, once R is determined.

$$F_{D,C} = \left|\frac{1}{4}(M + m_1)\left(4\ddot{x}_g + \frac{g}{R}x\right)\right| \tag{7}$$

$$F_{D,C} = \left|\frac{1}{2}(M + m_1)\left[2\ddot{x}_g + g\theta\, sgn(x)\right]\right| \tag{8}$$

With sloping angles of 3, 4, 6, and 8 degrees in the slope rolling range, the magnitudes of $F_{D,C}$ after excitations, i.e., $\ddot{x}_g = 0$, are correspondingly 256.83 N, 342.43 N, 513.65 N, and 684.87 N, of which the first two and the last two are smaller than and larger than their designed damping force magnitudes, respectively. It also means that for the designs with sloping angles of 3 and 4 degrees, if the magnitudes of $\ddot{x}_g$ during external disturbance are correspondingly larger than 0.030 g and 0.012 g with the same direction as x or larger than 0.082 g with the opposite direction to x, the motion between the superior and inferior bearing plates can still be in the slipping phase.

4. Numerical results and discussions

The horizontal maximum and residual displacement responses of CSD-3, CSD-6, VSD-36A, VSD-36B, VSD-63A, and VSD-63B subjected to ground motions of Groups 1, 2, and 3 are presented in Figs. 6-8, respectively, and those of CSD-4, CSD-8, VSD-48A, VSD-48B, VSD-84A, and VSD-84B subjected to ground motions of Groups 1, 2, and 3 are presented in Figs. 9-11, respectively. As for the horizontal maximum displacement responses subjected to ground motions of Group 1, another presentation, i.e., the horizontal maximum displacement responses versus PGV in a logarithm scale, is also provided for better observation. It is because the horizontal maximum displacement responses of sloped rolling-type seismic isolators have been numerically demonstrated to be almost linearly proportional to PGV in a logarithm scale (Hsu *et al*. 2021). In these figures, in addition to mean responses, 25th and 75th percentile responses are also provided for further statistical comparison. The numbers indicated in Figs. 6(a), 7(a), 8(a) and Figs. 6(b), 7(b), 8(b) represent the amounts of ground motions under which the displacement control performances of the models are better than those of CSD-3 and CSD-6 (their average responses are also presented), respectively. The numbers indicated in Figs. 9(a), 10(a), 11(a) and Figs. 9(b), 10(b), 11(b) represent the amounts of ground motions under which the displacement control performances of the models are better than those of CSD-4 and CSD-8 (their average responses are also presented), respectively. Since all the models are designed with the same curvature radius in the first transition range, the numerical results in the first transition range (including still at the equilibrium position if there are any) are contained in the figures and the following discussions. Note that the objective of this study is to numerically compare the merits and demerits of Design I and Design II models, rather than to design horizontal isolation displacement as small (or satisfactory) as possible for sloped rolling-type seismic isolators against the ground motion considered.

When subjected to ground motions of Group 1, as shown in Figs. 6(a) and 9(a), on average and in terms of amounts and distribution, CSD-3 and CSD-4, obviously, have better performances of suppressing horizontal

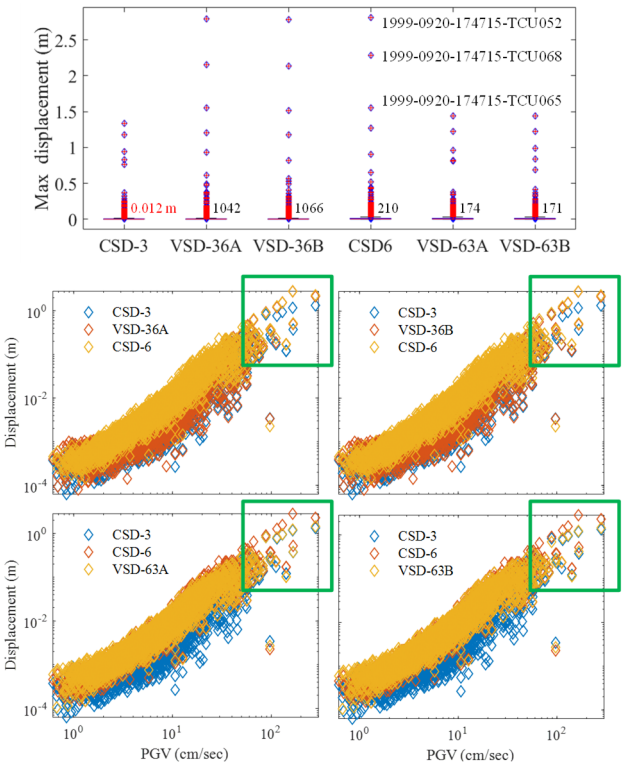

(a) Maximum displacement responses

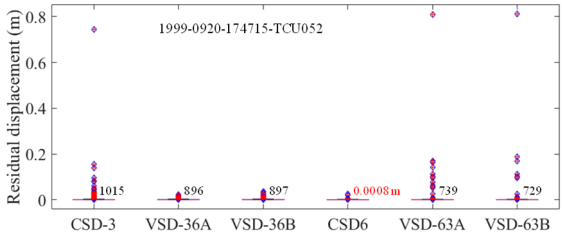

(b) Residual displacement responses

Fig. 6 Horizontal displacement responses of CSD-3, CSD-6, VSD-36A, VSD-36B, VSD-63A, and VSD-63B subjected to ground motions of Group 1

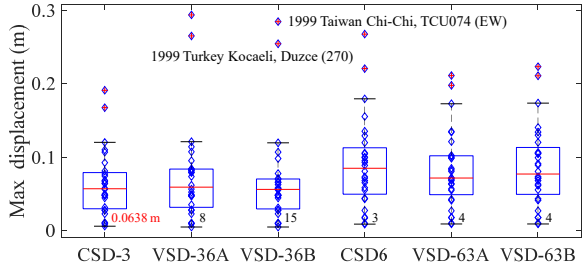

(a) Maximum displacement responses

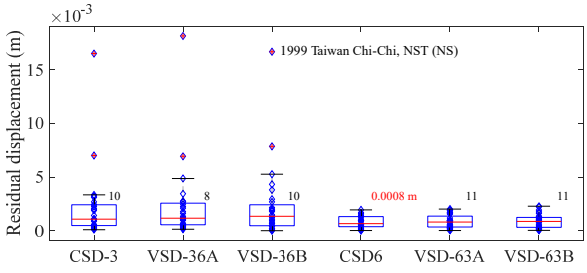

(b) Residual displacement responses

Fig. 7 Horizontal displacement responses of CSD-3, CSD-6, VSD-36A, VSD-36B, VSD-63A, and VSD-63B subjected to ground motions of Group 2

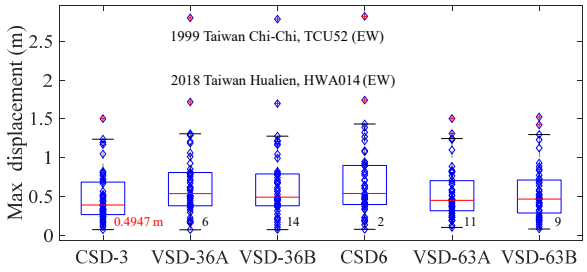

(a) Maximum displacement responses

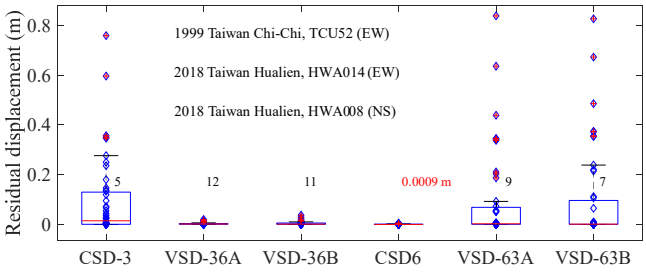

(b) Residual displacement responses

Fig. 8 Horizontal displacement responses of CSD-3, CSD-6, VSD-36A, VSD-36B, VSD-63A, and VSD-63B subjected to ground motions of Group 3

maximum displacement responses because of their larger damping force designs during the whole motion compared with the other models, while CSD-6 and CSD-8 have worse performances because of their smaller damping force designs. In other words, with the same horizontal acceleration control performance, adopting a smaller sloping angle (or larger damping force) design is more effective in suppressing horizontal isolation displacement than adopting a larger sloping angle (or smaller damping force) design. With the same reasons, the opposite tendency is observed for the re-centering performance, as shown in Figs. 6(b) and 9(b). As presented in Figs. 6(a) and 9(a), the Design I models, i.e., VSD-36A (VSD-48A) and VSD-36B (VSD-48B), have an almost comparable performance of suppressing horizontal maximum displacement responses to CSD-3 (CSD-4) when under a smaller horizontal isolation displacement demand, while the Design II models, i.e., VSD-63A (VSD-84A) and VSD-63B (VSD-84B), do when under a larger horizontal isolation displacement demand, as indicated by green squares. It is because of their larger damping force designs (as large as that for CSD-3 or CSD-4) in the first or second sloping range. Apparently, adopting a combination of sloping angles of 3 degrees and 6 degrees is better for suppressing horizontal isolation displacement than adopting a combination of sloping angles of 4 degrees and 8 degrees. Since most of ground motions of Group 1 are classified as far-field ground motions, which usually do not cause an excessive horizontal isolation displacement demand for seismic isolation design, it is of no surprise

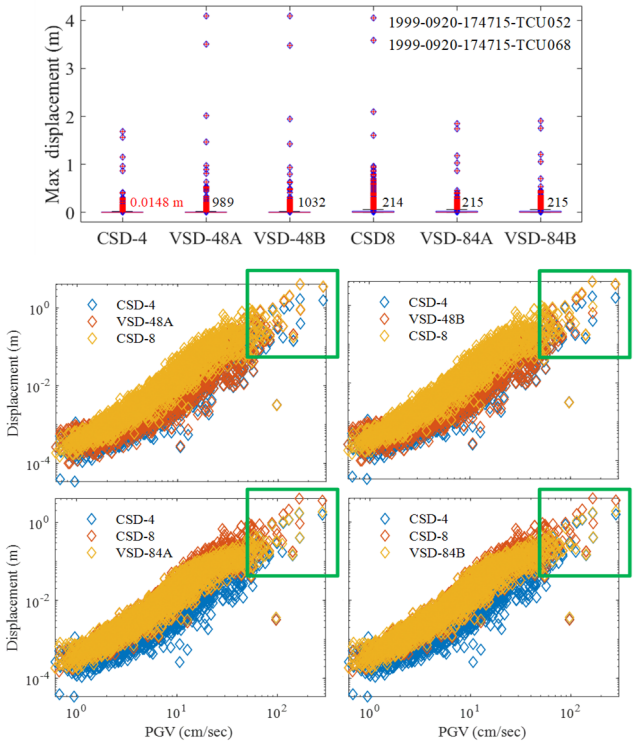

(a) Maximum displacement responses

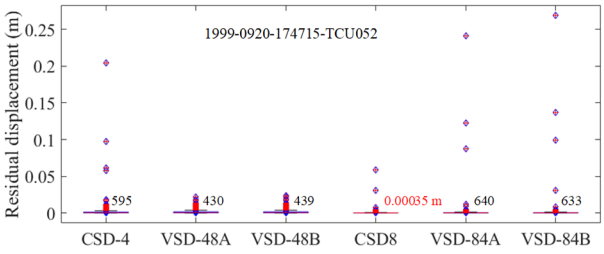

(b) Residual displacement responses

Fig. 9 Horizontal displacement responses of CSD-4, CSD-8, VSD-48A, VSD-48B, VSD-84A, and VSD-84B subjected to ground motions of Group 1

that the amounts of ground motions under which the Design I models perform better are much more than those under which the Design II models perform better. As presented in Figs. 6(b) and 9(b), on average, i.e., if some extremes are precluded, there is no significant discrepancies for the re-centering performances of different models. In terms of distribution, the residual displacement responses of the Design I models might not be as scattered as those of the Design II models. Apparently, adopting a combination of sloping angles of 4 degrees and 8 degrees for reducing residual displacement is better than adopting a combination of sloping angles of 3 degrees and 6 degrees.

To have further insight into the merits and demerits of Design I and II models, their responses subjected to ground motions of Group 2 and Group 3 are separately discussed and compared in the following. When subjected to ground motions of Group 2 (i.e., under the far-field ground motions), which usually do not cause an excessive horizontal isolation displacement demand for seismic isolation design, as presented in Figs. 7(a) and 10(a), on

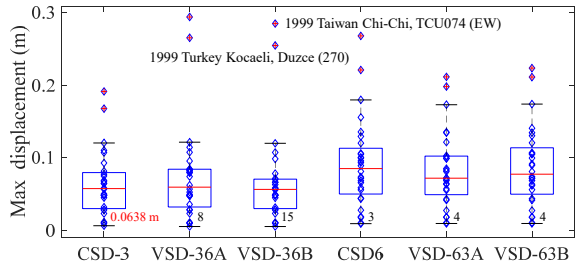

(a) Maximum displacement responses

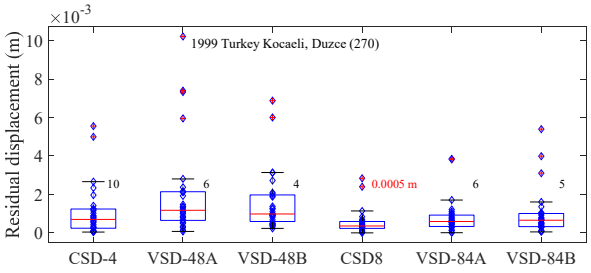

(b) Residual displacement responses

Fig. 10 Horizontal displacement responses of CSD-4, CSD-8, VSD-48A, VSD-48B, VSD-84A, and VSD-84B subjected to ground motions of Group 2

average and in terms of amounts and distribution of horizontal maximum displacement responses, the Design I models have almost comparable performances to CSD-3 or CSD-4 and have better performances than the Design II models, in particular of the models designed with a longer first slope rolling range (or the transition between the first and second slope rolling ranges occurs later), i.e., VSD-36B and VSD-48B. It is because of their larger damping force designs (as large as that for CSD-3 or CSD-4) in the first sloping range. It is of no surprise that the Design I and II

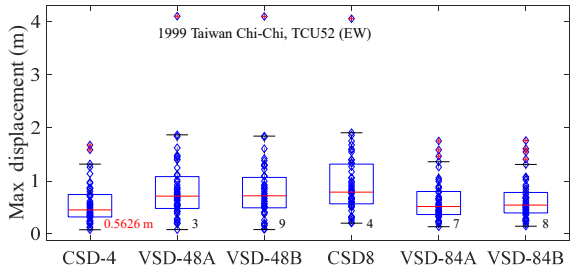

(a) Maximum displacement responses

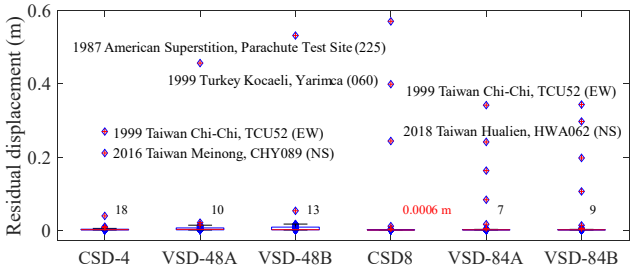

(b) Residual displacement responses

Fig. 11 Horizontal displacement responses of CSD-4, CSD-8, VSD-48A, VSD-48B, VSD-84A, and VSD-84B subjected to ground motions of Group 3

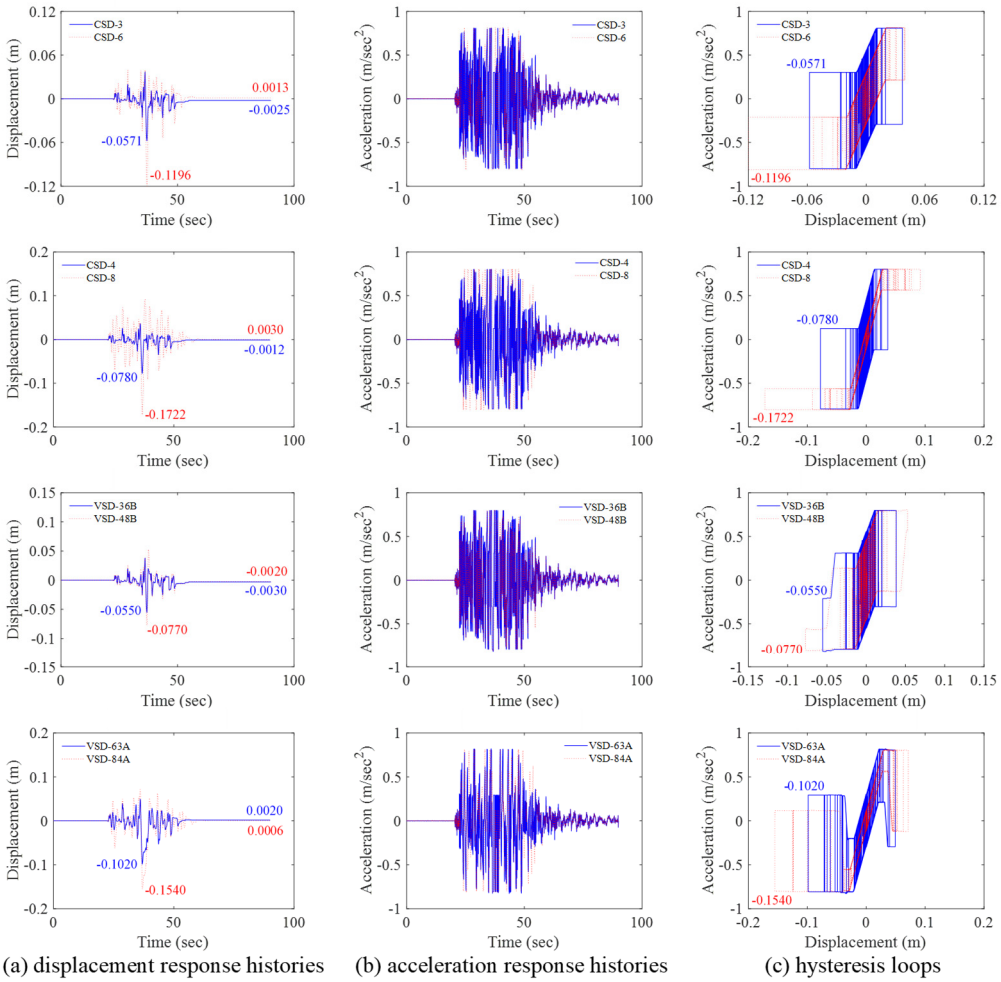

(a) displacement response histories (b) acceleration response histories (c) hysteresis loops

Fig. 12 Numerical results of CSD-3, CSD-4, CSD-6, CSD-8, VSD-36B, VSD-48B, VSD-63A, and VSD-84A under 1999 Taiwan Chi-Chi, TCU089 (EW) (Group 2)

models have better performances of suppressing horizontal maximum displacement responses than CSD-6 or CSD-8. All the models have the largest and second largest horizontal isolation displacement responses under 1999 Taiwan Chi-Chi, TCU074 (EW) and 1999 Turkey Kocaeli, Duzce (270), respectively. As for the re-centering performance, as shown in Figs. 7(b) and 10(b), on average and in terms of amounts and distribution, the almost opposite tendency is observed with the same reasons. Nevertheless, the Design II models have almost comparable re-centering performances to CSD-6 or CSD-8 and have superior re-centering performances to the Design I models, and the Design I models even perform worse than CSD-3 or CSD-4. Note that under the ground motions considered as shown in Figs. 7 and 10, regardless of any models, all the horizontal maximum displacement responses are controlled within 0.3 m, and most of residual displacement responses are very limited (an order of 10^{-4} to 10^{-3} meters), which are practically acceptable. Figs. 12-13 correspondingly present the displacement and acceleration response histories as well as the hysteresis loops of CSD-3, CSD-4, CSD-6, CSD-8, VSD-36B, VSD-48B, VSD-63A, and VSD-84A subjected to two ground motions of Group 2, i.e., 1999 Taiwan Chi-Chi, TCU089 (EW) and TCU074 (EW), under which all the models have smaller and larger horizontal isolation displacement responses, respectively. The numbers indicated in Figs. 12-13 represent the horizontal maximum and residual displacement responses of different models subjected to the ground motions. The results shown in these figures, of course, demonstrate again the observations and conclusions aforementioned. It is worth noting that the residual displacement responses of all the models under the ground motions are quite satisfactory. It is of no surprise for the satisfactory re-centering performances revealed by CSD-6 and CSD-8 since their calculated values of $F_{D,C}$ after excitations as per Eq. (8) are larger than their designed damping force magnitudes. As for VSD-63A and VSD-84A, their re-centering performances are still satisfactory since their horizontal isolation displacement responses at the end of the ground motions are within the first slope rolling range designed with sloping angles of 6 and 8 degrees, respectively. As for CSD-3, CSD-4, VSD-36B, and VSD-48B, since the magnitudes of $\ddot{x}_g$ at the end of the ground motions are large sufficiently to overcome their designed damping force magnitudes, their re-centering performances are also acceptable but not as good as those revealed by VSD-63A and VSD-84A.

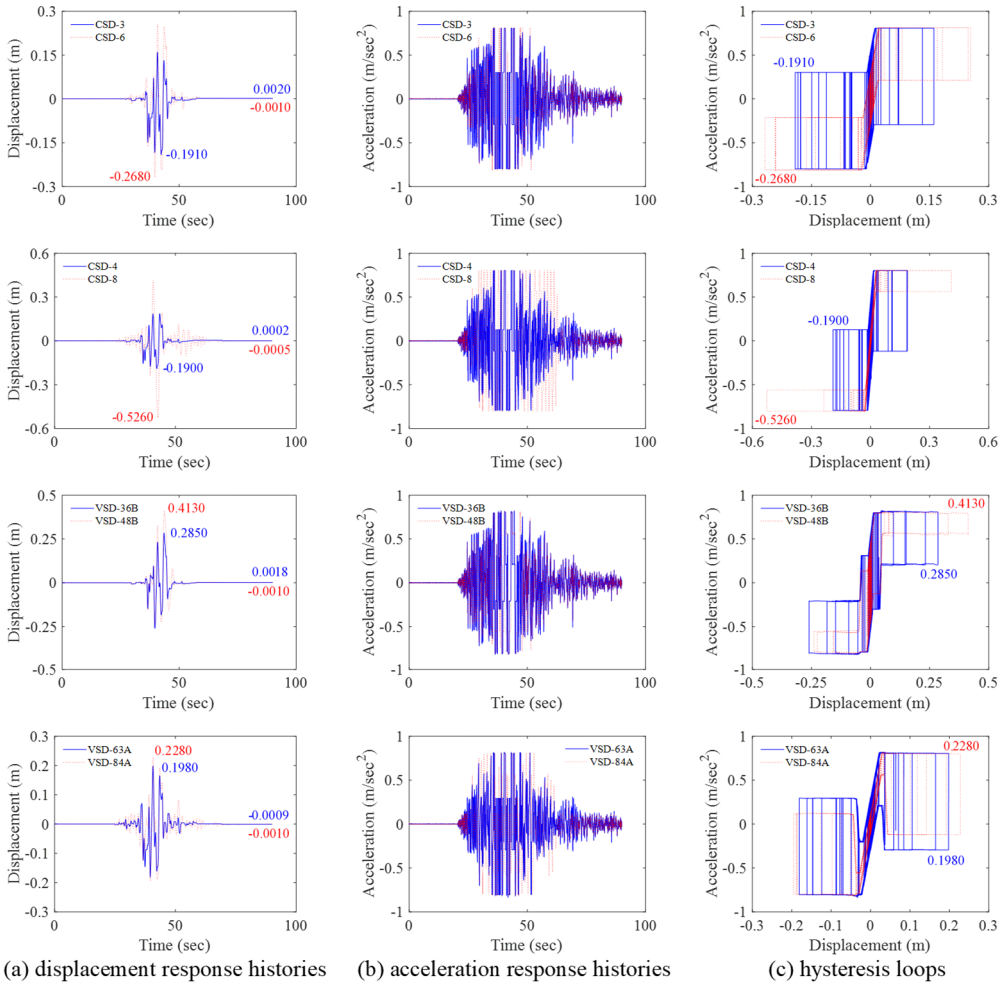

(a) displacement response histories (b) acceleration response histories (c) hysteresis loops

Fig. 13 Numerical results of CSD-3, CSD-4, CSD-6, CSD-8, VSD-36B, VSD-48B, VSD-63A, and VSD-84A under 1999 Taiwan Chi-Chi, TCU074 (EW) (Group 2)

When subjected to ground motions of Group 3 (i.e., under the pulse-like near-fault ground motions), which usually cause a considerable horizontal isolation displacement demand for seismic isolation design, as presented in Figs. 8(a) and 11(a), on average and in terms of amounts and distribution of horizontal maximum displacement responses, the Design II models, irrespective of being designed with a shorter or longer first slope rolling range, have almost comparable performances to CSD-3 or CSD-4 and have better performances than the Design I models. It is because of their larger damping force designs (as large as that for CSD-3 or CSD-4) in the second sloping range. It is of no surprise that the Design I and II models have better performances of suppressing horizontal maximum displacement responses than CSD-6 or CSD-8. All the models have the largest and second largest horizontal isolation displacement responses under 1999 Taiwan Chi-Chi, TCU052 (EW) and 2018 Taiwan Hualien, HWA014 (EW), respectively. As for the re-centering performance, as shown in Figs. 8(b) and 11(b), on average, there is no significant difference between the performances of the Design I and II models; in terms of amounts, the Design I models might be slightly better than the Design II models; in terms of distribution, the Design I and II models each have its advantage for the combinations of sloping angles of 3, 6 degrees and 4, 8 degrees. In general, the Design I and II models have almost comparable re-centering performances to CSD-6 (or CSD-8). Figs. 14-15 correspondingly present the displacement and acceleration response histories as well as the hysteresis loops of CSD-3, CSD-4, CSD-6, CSD-8, VSD-36B, VSD-48B, VSD-63A, and VSD-84A subjected to two ground motions of Group 3, i.e., 2018 Taiwan Hualien, TRB042 (EW) and 1999 Taiwan Chi-Chi, TCU052 (EW), under which all the models have smaller and larger horizontal isolation displacement responses, respectively. The numbers indicated in Figs. 14-15 represent the horizontal maximum and residual displacement responses of different models subjected to the ground motions. The results shown in these figures, of course, demonstrate again the observations and conclusions aforementioned. It is of no surprise for the satisfactory re-centering performances revealed by CSD-6 and CSD-8 since their calculated values of $F_{D,C}$ after excitations as per Eq. (8) are larger than their designed damping force magnitudes. When under a smaller horizontal isolation displacement demand, i.e., subjected to 2018 Taiwan Hualien, TRB042 (EW), the re-centering performances of all the models, except for CSD-3, are satisfactory since the

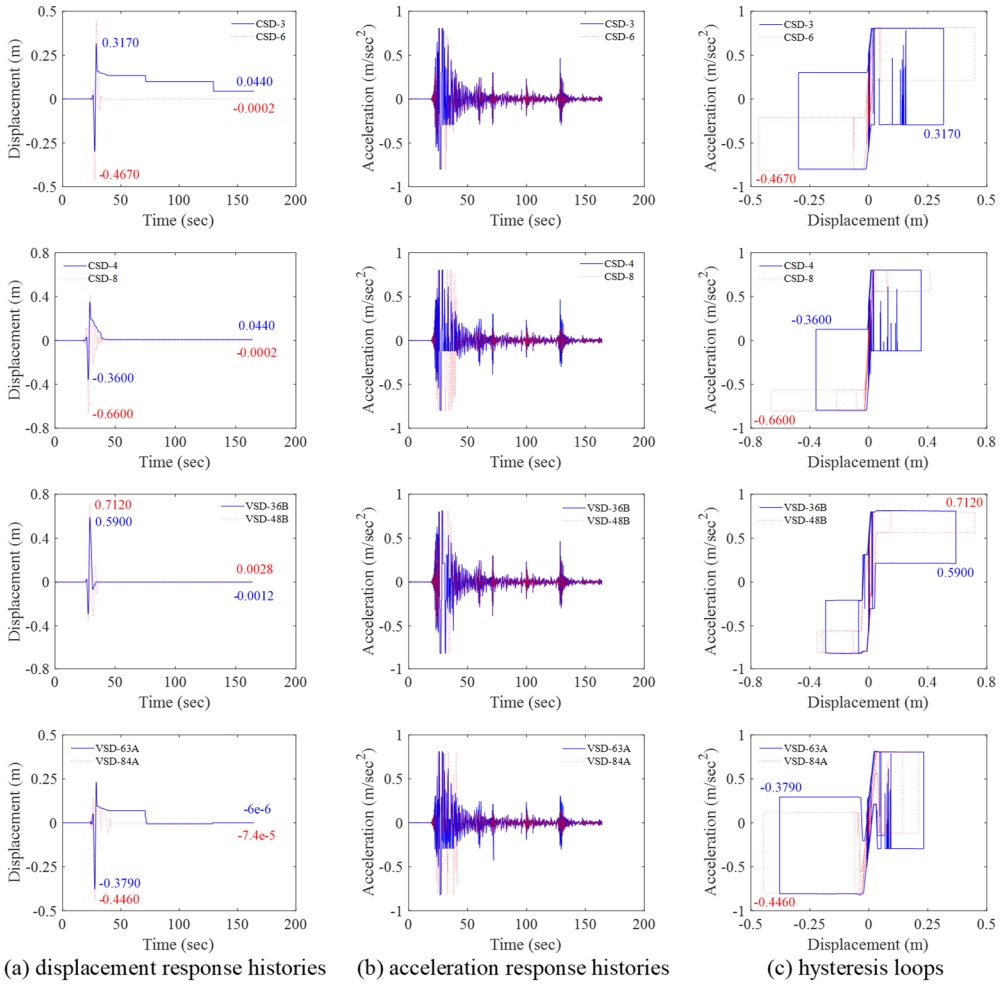

(a) displacement response histories (b) acceleration response histories (c) hysteresis loops

Fig. 14 Numerical results of CSD-3, CSD-4, CSD-6, CSD-8, VSD-36B, VSD-48B, VSD-63A, and VSD-84A under 2018 Taiwan Hualien, TRB042 (EW) (Group 3)

magnitudes of $\ddot{x}_g$ at the end of the ground motion are large enough to overcome their designed damping force magnitudes. However, when under a larger horizontal isolation displacement demand, i.e., subjected to 1999 Taiwan Chi-Chi, TCU052 (EW), the re-centering performances of CSD-3, CSD-4, VSD-63A, and VSD-84A become unacceptable, in particular of the first two, because of their excessive damping force designed. Under the circumstance, effectively controlling horizontal isolation displacement and reducing residual displacement as much as possible, rather than sacrificing horizontal isolation displacement to merely obtain a better re-centering performance, becomes more important. More precisely, on the basis of remaining the same horizontal acceleration control performance (e.g., 0.08 g assumed in the numerical study), instead of purely enlarging the constant damping force (e.g., CSD-3 in the numerical study), adopting Design II models, i.e., designed with stepwise decreased sloping angles and stepwise increased damping force with increasing horizontal isolation displacement (e.g., VSD-63A or VSD-63B in the numerical study), could be an alternative solution and better choice for reducing horizontal maximum and residual displacement as much as possible.

5. Conclusions

In this study, sloped rolling-type seismic isolators passively provided with stepwise variable sloping angles and damping force are numerically investigated and compared with those provided with a constant sloping angle and damping force. Some conclusions obtained from the numerical results and comparisons are made as follows.

- On the premise of remaining the same horizontal acceleration control performance, sloped rolling-type seismic isolators designed with a constant sloping angle and damping force might be unable to well control their horizontal maximum and residual displacement responses simultaneously. More precisely, the increase of damping force or the decrease of sloping angles will indeed lead to a decrease in horizontal isolation displacement but meanwhile will also cause an increase in residual displacement. In the conventional thought, to have acceptable displacement control performances under diverse seismic demands, the strategy of sacrificing acceleration control performances is usually adopted. Therefore, in this study, the ideas of stepwise

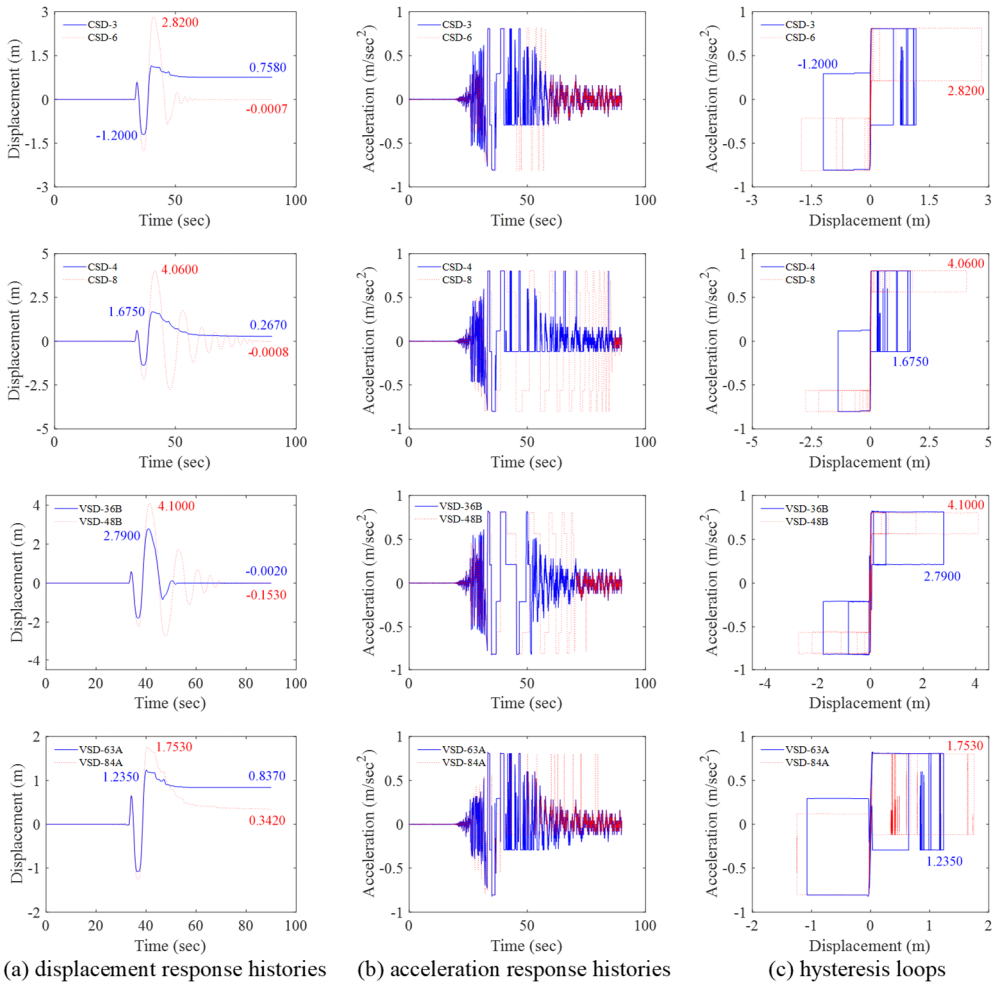

(a) displacement response histories (b) acceleration response histories (c) hysteresis loops

Fig. 15 Numerical results of CSD-3, CSD-4, CSD-6, CSD-8, VSD-36B, VSD-48B, VSD-63A, and VSD-84A under 1999 Taiwan Chi-Chi, TCU052 (EW) (Group 3)

variable sloping angles and damping force are proposed to be implemented into sloped rolling-type seismic isolators. By means of being subjected to a great number of ground motions and further classifying ground motions into far-field and pulse-like near-fault ones, the horizontal displacement control performances of the isolators, in terms of maximum and residual displacement responses, are thoroughly and statistically compared and discussed. It is emphasized again that the purpose of the diverse ground motions considered and the models designed in this study is to obtain wide-ranging seismic responses of the models, rather than to passively reduce their seismic responses as much as possible or to propose their optimum design approaches.

- In addition to two different design models provided with stepwise increased sloping angles and stepwise decreased damping force as well as stepwise decreased sloping angles and stepwise increased damping force with increasing horizontal isolation displacement, correspondingly denoted as Designs I and II in this study, earlier and later transitions between two different sloping angles and damping force, correspondingly denoted as A and B in this study, are also adopted as one of variable parameters for the numerical analysis. Sloped rolling-type seismic isolators designed with four constant sloping angles, 3, 4, 6, and 8 degrees are adopted as the counterparts, of which the first two can make the isolators always remain the slipping phase even without being subjected to external disturbance, while the last two cannot. The numerical and statistical comparison results indicate that with the same horizontal acceleration control performance, adopting Design I, which has a larger energy dissipation capability at smaller horizontal isolation displacement, is more effective in reducing horizontal isolation displacement than adopting Design II under far-field ground motions, which usually do not cause an excessive horizontal isolation displacement demand for seismic isolation design. On the contrary, adopting Design II, which has a larger energy dissipation capability at larger horizontal isolation displacement, is better than adopting Design I under pulse-like near-fault ground motions, which usually cause a considerable horizontal isolation displacement demand for seismic isolation design. Under the far-field ground

motions considered, all the displacement responses of either Designs I or II are practically acceptable. As for the re-centering performance, although the difference between adopting Designs I and II might not be very significant because the excitation magnitudes at the end of most of the ground motions considered are large sufficiently, it can still be observed that Design II has an advantage over Design I when the horizontal isolation displacement responses at the end of the ground motions are within the first slope rolling range designed with a larger sloping angle. Thus, to have acceptable displacement control performances and without scarifying acceleration control performances under diverse seismic demands, compared with adopting the designs with constant parameters and Design I, adopting Design II could be an alternative solution and better choice.

- The current conclusions, indeed, are made simply based on the numerical results of limited combinations of design parameters and only one acceleration performance objective. To have more convincing results, more combinations of design parameters and more acceleration performance objectives might be needed to be further studied in a numerical or experimental manner in the future.
- A series of experimental researches previously conducted by Wang *et al*. (2014, 2017) have presented that an arc design existing between two discontinuous slopes can mechanically exhibit the linearly elastic behavior. In addition, it has been experimentally demonstrated that the linearly variable damping force can be passively realized through designing one surface sliding against the other surface behind which the installed linear spring modules are compressed with shortening linearly proportional to horizontal isolation displacement (Wang *et al*. 2020). Therefore, the design concept proposed in this study, stepwise variable sloping angles and damping force with increasing horizontal isolation displacement, could be practically feasible. Although the mechanisms of stepwise variable sloping angles and damping force have been separately verified in past experimental researches, further experimental demonstration of the whole system integrated with the two mechanisms is still required. After numerically demonstrating the effectiveness of the proposed design concept and its advantages over other passive design cases in this study, the relevant tests of the whole system will be schemed and conducted in the future.

Acknowledgments

The study was financially aided by the Ministry of Science and Technology (MOST) of Taiwan [104-2221-E-492-021-]. The support is greatly acknowledged.

References

Abdollahzadeh, G. and Darvishi, R. (2017), "Cyclic behavior of DCFP isolators with elliptical surfaces and different frictions", *Struct. Eng. Mech., Int. J.*, **64**(6), 731-736. https://doi.org/10.12989/sem. 2017.64.6.731

Baker, J.W. (2007), "Quantitative classification of near-fault ground motions using wavelet analysis", *Bull. Seismol. Soc. Am.*, **97**(5), 1486-1501. https://doi.org/10.1785/0120060255

Calvi, P.M., Moratti, M. and Calvi, G.M. (2008), "Seismic isolation devices based on sliding between surfaces with variable friction coefficient", *Earthq. Spectra*, **32**(4), 2291-2315. https://doi.org/10.1193/ 091515EQS139M

Chang, S.P., Makris, N., Whittaker, A.S. and Thompson, A.C.T. (2002), "Experimental and analytical studies on the performance of hybrid isolation systems", *Earthq. Eng. Struct. Dyn.*, **31**(2), 421-443. https://doi.org/10.1002/eqe.117

Chen, P.C. and Wang, S.J. (2016), "Improved control performance of sloped rolling-type isolation devices using embedded electromagnets", *Struct. Control Health Monitor.*, **24**(1), e1853. https://doi.org/ 10.1002/stc.1853

Chen, P.C., Hsu S.C., Zhong, Y.J. and Wang, S.J. (2019), "Real-time hybrid simulation of smart base-isolated raised floor systems for high-tech industry", *Smart Struct. Syst., Int. J.*, **23**(1), 91-106. http://dx.doi.org/10.12989/sss.2019.23.1.091

Chopra, A.K. and Chintanapakdee, C. (2014), "Comparing response of SDF systems to near-fault and far-fault earthquake motions in the context of spectral regions", *Earthq. Eng. Struct. Dyn.*, **30**(12), 1769-1789. https://doi.org/10.1002/eqe.92

Constantinou, M.C., Mokha, A. and Reinhorn, A. (1990), "Teflon bearings in base isolation II: modeling", *J. Struct. Eng. ASCE*, **116**(2), 455-474. https://doi.org/10.1061/(ASCE)0733-9445 (1990)116:2(455)

Feng, M.Q., Shinozuka, M. and Fujii, S. (1993), "Friction-controllable sliding isolation system", *J. Eng. Mech. ASCE*, **119**(9), 1845-1864. https://doi.org/10.1061/(ASCE)0733-9399(1993)119: 9(1845)

Fenz, D.M. and Constantinou, M.C. (2006), "Behaviour of the double concave friction pendulum bearing", *Earthq. Eng. Struct. Dyn.*, **35**(11), 1403-1424. https://doi.org/10.1002/eqe.589

Fenz, D.M. and Constantinou, M.C. (2008), "Modeling triple friction pendulum bearings for response-history analysis", *Earthq. Spectra*, **24**(4), 1011-1028. https://doi.org/10.1193/1.2982531

Ghobarah, A. (2001), "Performance-based design in earthquake engineering: state of development", *Eng. Struct.*, **23**(8), 878-884. https://doi.org/10.1016/S0141-0296(01)00036-0

Harvey, Jr. P.S. and Kelly, K.C. (2016), "A review of rolling-type seismic isolation: historical development and future directions", *Eng. Struct.*, **125**, 521-531. https://doi.org/10.1016/j.engstruct.2016.07.031

He, W.L., Agrawal, A.K. and Yang, J.N. (2003), "Novel semiactive friction controller for linear structures against earthquakes", *J. Struct. Eng. ASCE*, **129**(7), 941-950. https://doi.org/10.1061/ (ASCE)0733-9445(2003)129:7(941)

Hsu, T.Y., Huang, C.H. and Wang, S.J. (2021), "Early adjusting damping force for sloped rolling-type seismic isolators based on earthquake early warning information", *Earthq. Struct., Int. J.*, **20**(1), 39-53. http://dx.doi.org/10.12989/eas.2021.20.1.039

Hwang, J.S., Huang, Y.N., Hung, Y.H. and Huang, J.C. (2004), "Applicability of seismic protective systems to structures with vibration sensitive equipment", *J. Struct. Eng. ASCE*, **130**(11), 1676-1684. https://doi.org/10.1061/(ASCE)0733-9445(2004)130:11(1676)

Iemura, H., Igarashi, A., Pradono, M.H. and Kalantari, A. (2019), "Negative stiffness friction damping for seismically isolated

structures", *Struct. Control Health Monitor.*, **13**(2-3), 775-791. https://doi.org/10.1002/stc.111

Jangid, R.S. (2017), "Optimum friction pendulum system for near-fault motions", *Eng. Struct.*, **27**(3), 349-359. https://doi.org/10.1016/j.engstruct.2004.09.013

Kumar, M., Whittaker, A.W. and Constantinou, M.C. (2015), "Characterizing friction in sliding isolation bearings", *Earthq. Eng. Struct. Dyn.*, **44**(9), 1409-1425. https://doi.org/10.1002/ eqe.2524

Lee, G.C., Ou, Y.C., Niu, T., Song, J. and Liang, Z. (2010), "Characterization of a roller seismic isolation bearing with supplemental energy dissipation for highway bridges", *J. Struct. Eng. ASCE*, **136**(5), 502-510. https://doi.org/10.1061/(ASCE)ST.1943-541X.0000136

Liu, Y., Matsuhisa, H. and Utsuno, H. (2008), "Semi-active vibration isolation system with variable stiffness and damping control", *J. Sound Vib.*, **313**(1-2), 16-28. https://doi.org/10.1016/ j.jsv.2007.11.045

Lu, L.Y., Lin, G.L. and Kuo, T.C. (2008), "Stiffness controllable isolation system for near-fault seismic isolation", *Eng. Struct.*, **30**(3), 747-765. https://doi.org/10.1016/j.engstruct.2007.05.022

Lu, L.Y., Lee, T.Y., Juang, S.Y. and Yeh, S.W. (2013), "Polynomial friction pendulum isolators (PFPIs) for building floor isolation: An experimental and theoretical study", *Eng. Struct.*, **56**, 970-982. https://doi.org/10.1016/j.engstruct.2013.06.016

Makris, N. and Chang, S.P. (2000), "Effect of viscous, viscoplastic and friction damping on the response of seismic isolated structures", *Earthq. Eng. Struct. Dyn.*, **29**(1), 85-107. https://doi.org/10.1002/(SICI)1096-9845(200001)29:1<85::AID-EQE902>3.0.CO;2-N

Narasimhan, S. and Nagarajaiah, S. (2005), "A STFT semiactive controller for base isolated buildings with variable stiffness isolation systems", *Eng. Struct.*, **27**(4), 514-523. https://doi.org/10.1016/j.engstruct.2004.11.010

Narasimhan, S. and Nagarajaiah, S. (2006), "Smart base isolated buildings with variable friction systems: H∞ controller and SAIVF device", *Earthq. Eng. Struct. Dyn.*, **35**(8), 921-942. https://doi.org/10.1002/eqe.559

Ozbulut, O.E. and Hurlebaus, S. (2010), "Fuzzy control of piezoelectric friction dampers for seismic protection of smart base isolated buildings", *Bull. Earthq. Eng.*, **8**(6), 1435-1455. https://doi.org/10.1007/s10518-010-9187-5

Ozbulut, O.E., Bitaraf, M. and Hurlebaus, S. (2011), "Adaptive control of base-isolated structures against near-field earthquakes using variable friction dampers", *Eng. Struct.*, **33**(12), 3143-3154. https://doi.org/10.1016/j.engstruct.2011.08.022

Panchal, V.R. and Jangid, R.S. (2008), "Variable friction pendulum system for near-fault ground motions", *Struct. Control Health Monitor.*, **15**(4), 568-584. https://doi.org/10.1002/stc.216

Ponzo, F.C., Cesare, A.D., Leccese, G. and Nigro, D. (2017), "Shake table testing on restoring capability of double concave friction pendulum seismic isolation systems", *Earthq. Eng. Struct. Dyn.*, **46**(14), 2337-2353. https://doi.org/10.1002/eqe.2907

Shahbazi, P. and Taghikhany, T. (2017), "Sensitivity analysis of variable curvature friction pendulum isolator under near-fault ground motions", *Smart Struct. Syst., Int. J.*, **20**(1), 23-33. https://doi.org/10.12989/sss. 2017.20.1.023

Shahi, S.K. and Baker, J.W. (2014), "An efficient algorithm to identify strong-velocity pulses in multicomponent ground motions", *Bull. Seismol. Soc. Am.*, **104**(5), 2456-2466. http://dx.doi.org/10.1785/0120130191

Tadjbakhsh, I. and Lin, B.C. (1987), "Displacement-proportional friction (DPF) in base isolation", *Earthq. Eng. Struct. Dyn.*, **15**(7), 799-813. https://doi.org/10.1002/eqe.4290150702

Tsai, M.H., Wu, S.Y., Chang, K.C. and Lee, G.C. (2007), "Shaking table tests of a scaled bridge model with rolling type seismic isolation bearings", *Eng. Struct.*, **29**(9), 694-702. https://doi.org/10.1016/j.engstruct.2006.05.025

Wang, S.J., Hwang, J.S., Chang, K.C., Shiau, C.Y., Lin, W.C., Tsai, M.S., Hong, J.X. and Yang, Y.H. (2014), "Sloped multi-roller isolation devices for seismic protection of equipment and facilities", *Earthq. Eng. Struct. Dyn.*, **43**(10), 1443-1461. https://doi.org/10.1002/eqe.2404

Wang, S.J., Yu, C.H., Lin, W.C., Hwang, J.S. and Chang, K.C. (2017), "A generalized analytical model for sloped rolling-type seismic isolators", *Eng. Struct.*, **138**, 434-446. https://doi.org/10.1016/j.engstruct.2016.12.027

Wang, S.J., Yu, C.H., Cho, C.Y. and Hwang, J.S. (2019), "Effects of design and seismic parameters on horizontal displacement responses of sloped rolling-type seismic isolators", *Struct. Control Health Monitor.*, **26**(5). https://doi.org/10.1002/stc.2342

Wang, S.J., Sung, Y.L. and Hong, J.X. (2020), "Sloped rolling-type bearings designed with linearly variable damping force", *Earthq. Struct., Int. J.*, **19**(2), 129-144. http://dx.doi.org/10.12989/eas.2020. 19.2.129

Wei, B., Wang, P., He, X., Zhang, Z. and Chen, L. (2017), "Effects of friction variability on a rolling-damper-spring isolation system", *Earthq. Struct., Int. J.*, **13**(6), 551-559. https://doi.org/10.12989/eas. 2017.13.6.551

Yurdakul, M. and Ates, S. (2018), "Stochastic responses of isolated bridge with triple concave friction pendulum bearing under spatially varying ground motion", *Struct. Eng. Mech., Int. J.*, **65**(6), 771-784. https://doi.org/10.12989/sem.2018.65.6.771

BS